Recursive Green-function study of Wannier - Stark effect in tight-binding systems

1997 J. Phys.: Condens. Matter 9 6371

(http://iopscience.iop.org/0953-8984/9/30/006)

J. Phys.: Condens. Matter **9** (1997) 6371–6382. Printed in the UK PII: S0953-8984(97)82502-7

Recursive Green-function study of Wannier–Stark effect in tight-binding systems

S G Davison†‖, R A English†, Z L Mišković†¶, F O Goodman†‖, A T Amos‡+ and B L Burrows§+

† Department of Applied Mathematics, University of Waterloo, Waterloo, Ontario N2L 3G1, Canada

‡ Department of Computer Science & Applied Mathematics, Aston University, Birmingham B4 7ET, UK

§ Department of Mathematics, Staffordshire University, Beaconside, Stafford ST18 0AD, UK

Received 11 March 1997, in final form 16 June 1997

Abstract. The Wannier–Stark effect in electrified tight-binding systems is investigated, via the recursive Green-function technique, which involves repeated use of the Dyson equation. Green functions for finite, semi-infinite and infinite systems are generated in the site representation in the form of continued fractions, which are then expressed analytically as ratios of Bessel functions. The local densities of states at the surface and in the bulk are presented and their dependence on the applied field discussed.

1. Introduction

Zener's pioneering work on dielectric breakdown [1] provided the first glimpse into the challenging world of electrified solids. However, more than a quarter of a century had to elapse before the notion of the *Stark ladder* was proposed by Wannier [2] in 1960. The ensuing controversy over the existence of *Wannier–Stark ladders* (WSL) in multi-band structures was reviewed and discussed in some detail [3].

The *tight-binding* (TB) approximation [4] has been widely used to treat WSLs in one- and two-band systems, since it reflects the salient physical aspects of real crystals. More recently, a perturbative investigation of WSLs in infinite diatomic crystals was undertaken by Zhao [5], who found that, in the two-band energy spectrum, the WSLs were interspaced. For finite crystals, he also found that the interband matrix elements were non-zero [6].

Optical absorption in electrified δ-doped semiconductors was examined by Ahn [7]. Solving the Schrödinger equation for a V-shaped *quantum well* (QW) in an electric field, he predicted wide-range tuning of intersubband absorption by controlling planar doping, and also the presence of red rather than blue shifts associated with electro-adsorption in ordinary QWs. In a comparative study, Anwar and Jahan [8] performed a self-consistent calculation of the density of states of double-barrier QW structures in magnetic and electric fields, and described the energy redistribution and a phase-breaking mechanism. An electrified multi-band QW, in the form of a finite *Kronig–Penney* (KP) structure, was used by Vrubel

‖ Also with the Department of Physics, University of Waterloo, and the Guelph-Waterloo Program for Graduate Work in Physics.

¶ On leave from the Institute for Nuclear Sciences, Belgrade, Serbia, Yugoslavia.

+ Also affiliated with the Department of Applied Mathematics, University of Waterloo.

0953-8984/97/306371+12$19.50

and Borzdov [9] in their treatment of the gradual transition from the *quantum confined Stark effect* (QCSE) to the WS quantization. Stark localization and mixing phenomena between different WSLs in coupled QWs were reported by Sari *et al* [10], who found that at intermediate WSL values a certain degree of carrier wavefunction delocalization exists, while at large values the WSL states become localized inside individual QWs and a combined band structure occurs.

Experimentally, Cohen *et al* [11] investigated the optical properties of a narrow-band GaAs/Al_x $Ga_{1-x}As$ *superlattice* and observed a modified WSL with both positive and negative orders appearing above the zero-order transition. QCSE in InGaAs/GaAs QWs under high electric fields was studied by Kavaliauskas *et al* [12] using photocurrent and electroreflectance spectroscopies. Evidence of exciton quenching and carrier tunnelling out of the QWs was obtained, while coupling between quasi-bound and continuum states resulted in an absorption increase below the barrier band gap.

Over the years, a large literature has accumulated on the WSL effect, so it is somewhat surprising to find that the number of papers devoted to the *Green function* (GF) formulation of the problem appears to be rather sparse. In a series of papers, Lukes and his co-workers [13] developed a time-independent method of calculating the single-particle GF, in terms of the corresponding Feynman propagator [14], for a δ-potential in a uniform electric field, which enabled exact expressions to be derived formally for the density of states and energy levels of an electrified *Dirac-delta comb* potential. Moyer [15], in his GF treatment, invoked first-order perturbation theory to describe the motion of an electron in an infinite, electrified KP lattice. Recently, Dolcher *et al* [16] reported a real-space GF numerical analysis of WSLs based on a modified *Lanczos iterative procedure*, which was applied to one-dimensional, one- and two-band TB systems. Meanwhile, the GF technique in the site representation was employed by Gvozdikov [17] to discuss the analogy between the *Landau spectrum* of a Bloch electron in a two-dimensional anisotropic lattice and the WSL.

In the present article, we take advantage of the recent advances made in TBGF methodology. Specifically, we exploit the *continued fraction* (CF) aspect of the recursion method [18] and develop an analytical GF on an *atom-by-atom* basis, in a similar fashion to the *causal-surface* GF approach of Pendry *et al* [19]. Thus, the method may be regarded as a mathematical means of crystal growth.

2. Methodology

Consider a monatomic chain of $(N+1)$ atoms, numbered $n \in (0, N)$, whose site (bond) energy is $\alpha(\beta)$. Let the gradient of the imposed electric field be γ, so that $\Gamma = \gamma a$ is the potential energy of the field, a being the chain atomic spacing. Assuming that the field perturbs the site energy of the atom n by an amount $n\Gamma$, then, within the TB approximation, the Schrödinger equation takes the form of the *Bessel* finite-difference equation [4]

$$Z_n c_n = c_{n+1} + c_{n-1} \tag{1}$$

where, in *dimensionless reduced notation*,

$$Z_n = 2(X - nF) \qquad X = (E - \alpha)/2\beta \qquad F = \Gamma/2\beta. \tag{2}$$

We now proceed to *construct* the GF of the chain-field system from its *atomic constituents* by means of the successive use of the *Dyson equation* [20]. Starting with the *zero-atom* end, we build the chain atom-by-atom up to the n-atom. Concomitantly, we begin from the *N-atom* end and build atom-by-atom to the $(n+1)$-atom. Finally, we join

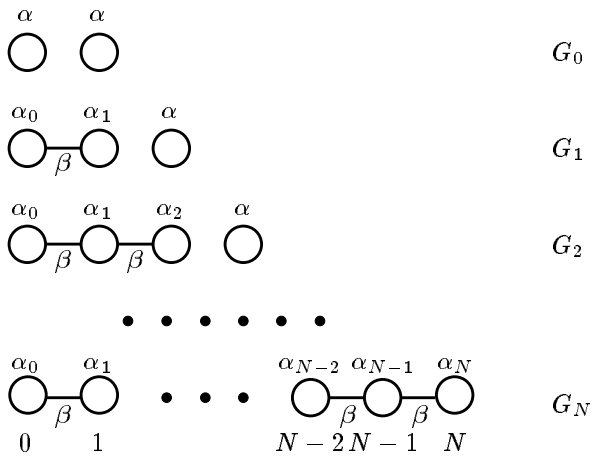

Figure 1. Diagrammatic representation of Green-function propagators along atomic chain of site (bond) energy α (β), with $\alpha_n = \alpha + n\Gamma$ at site n in field Γ.

the two chains, by means of the *bond-projection operator*

$$V = \beta\,(|n\rangle\langle n+1| + |n+1\rangle\langle n|)\,. \tag{3}$$

At the *0-atom* end, we have initially two *isolated* atoms (figure 1), whose Greenian is

$$G_0 = (|0\rangle\langle 0| + |1\rangle\langle 1|)\,(E-\alpha)^{-1}. \tag{4}$$

On forming the β-bond between the atoms 0 and 1, and applying the field F (figure 1), the Dyson equation

$$G_1 = G_0 + G_0 V_1 G_1 \tag{5}$$

gives G_1 in terms of G_0 and the perturbation potential

$$V_1 = \beta\,(|0\rangle\langle 1| + |1\rangle\langle 0|) + \Gamma|1\rangle\langle 1|. \tag{6}$$

Inserting (6) into (5), and performing some algebra, leads to the Greenian matrix element at the first atom, viz,

$$G_1(1) = \left[G_0(1)^{-1} - \Gamma - \beta^2 G_0(0)\right]^{-1} \tag{7}$$

where $G_m(m) \equiv G_m(m,m)$. Following this same recipe for atom 2, we arrive at

$$G_2(2) = \left\{G_1(2)^{-1} - 2\Gamma - \beta^2[G_0(1)^{-1} - \Gamma - \beta^2 G_0(0)]^{-1}\right\}^{-1}. \tag{8}$$

Since

$$G_{m-1}(m)^{-1} = (E-\alpha) \qquad \forall\ m \neq 0 \tag{9}$$

by (4), mathematical induction leads to the *CF form* [21]

$$\beta G_n(n) = \frac{1}{Z_n} - \frac{1}{Z_{n-1}} - \frac{1}{Z_{n-2}} - \cdots \frac{1}{Z_1 - Z_0^{-1}} \tag{10}$$

for the n-site GF. Similarly, starting at the N-*atom* end, and working to the *left*, we obtain the CF

$$\beta G_{n+1}(n+1) = \frac{1}{Z_{n+1}} - \frac{1}{Z_{n+2}} - \cdots \frac{1}{Z_{N-1} - Z_N^{-1}} \tag{11}$$

for the $(n+1)$-site CF.

At this juncture, we connect the above two chains via (3) and (5), where

$$G_0 = G_n + G_{n+1}. \tag{12}$$

Using the general form of (4), in conjunction with (3), (5) and (12), we arrive at

$$\beta G(n) = \left[\beta^{-1} G_n(n)^{-1} - \beta G_{n+1}(n+1)\right]^{-1}. \tag{13}$$

Inserting (10) and (11) into (13), we have

$$\beta G_N(n) = \left[\left(\frac{1}{Z_n} - \frac{1}{Z_{n-1}} - \cdots \frac{1}{Z_1 - Z_0^{-1}}\right)^{-1} - \left(\frac{1}{Z_{n+1}} - \frac{1}{Z_{n+2}} - \cdots \frac{1}{Z_{N-1} - Z_N^{-1}}\right)\right]^{-1} \tag{14}$$

which gives the *diagonal* elements of the Greenian matrix for the *finite* chain $(0, N)$. Proceeding further, (5) and (6) enable the general expression for the *off-diagonal* terms to be derived, i.e.

$$\beta G_n(0, n) = \prod_{m=0}^{n} \beta G_m(m). \tag{15}$$

Rewriting (1) as the 3-term *recursion relation*

$$c_n = b_n c_{n-1} + a_n c_{n-2} \qquad a_n \neq 0 \ \forall \ n \tag{16}$$

then, if $\{c_n\}_{n=1}^{\infty}$ is a *minimal* solution set of (16), a second, linearly independent, *dominant* set, $\{c'_n\}_{n=1}^{\infty}$, will also exist. On choosing the minimal solution set, so that

$$\lim_{n\to\infty} \left(\frac{c_n}{c'_n}\right) \to 0 \tag{17}$$

Pincherle's theorem [21] states that the CF

$$\mathop{\mathcal{K}}_{m=1}^{\infty}(a_m; b_m) = -\frac{c_0}{c_{-1}} \tag{18}$$

where

$$\mathop{\mathcal{K}}_{m=1}^{\infty}(a_m; b_m) = \frac{a_1}{b_1} + \frac{a_2}{b_2} + \cdots \tag{19}$$

For a *finite* chain of N atoms, (19) becomes the *N-approximant*

$$\mathop{\mathcal{K}}_{m=1}^{N}(a_m; b_m) = \frac{a_1}{b_1} + \frac{a_2}{b_2} + \cdots \frac{a_N}{b_N} \tag{20}$$

which may be written as

$$\mathop{\mathcal{K}}_{m=1}^{N}(a_m; b_m) = \frac{c'_0 c_N - c_0 c'_N}{-c'_{-1} c_N + c_{-1} c'_N}. \tag{21}$$

Note, in the limit as $N \to \infty$, (21) reduces to (18) via (17). A comparison of (16) and (1) shows that

$$a_m = -1 \qquad b_m = Z_{m-1} \tag{22}$$

while the *Bessel-function* (BF) form of (1) means that the minimal (dominant) solution is the BF of the first (second) kind. Thus,

$$\begin{aligned} c_n &= J_{\nu+n}(x) \\ c'_n &= Y_{\nu+n}(x) \end{aligned} \tag{23}$$

where

$$\nu = xX \qquad x = -F^{-1}. \tag{24}$$

In view of (21) and (23), evaluating (14) at the $n = 0$ site yields [22]

$$\beta G_N(0) = -\mathop{\mathcal{K}}_{m=0}^{N}(-1; Z_m) = -\frac{J_{\nu+N}(x)Y_\nu(x) - J_\nu(x)Y_{\nu+N}(x)}{J_{\nu-1}(x)Y_{\nu+N}(x) - J_{\nu+N}(x)Y_{\nu-1}(x)} \tag{25}$$

for a *finite* chain. In the limit of $N \to \infty$, (25) reduces to

$$\beta G_\infty(0) = -\mathop{\mathcal{K}}_{m=0}^{\infty}(-1; Z_m) = \frac{J_\nu(x)}{J_{\nu-1}(x)} \tag{26}$$

via (18) and (23), for a *semi-infinite* chain.

Turning to the *infinite* chain, for which $(0, N) \to (-\infty, \infty)$ in (14), we find

$$\begin{aligned} \beta G^\infty(n) = \Bigg[&\left(\frac{1}{Z_n} - \frac{1}{Z_{n-1}} - \cdots \frac{1}{Z_{-N}} - \cdots \right)^{-1} \\ &- \left(\frac{1}{Z_{n+1}} - \frac{1}{Z_{n+2}} - \cdots \frac{1}{Z_N} - \cdots \right) \Bigg]^{-1}. \end{aligned} \tag{27}$$

In the *zero-field* situation, $Z_n = Z_0 = 2X$ by (2), whence, (27) becomes

$$\beta G^\infty(n) = \left[\left(\frac{1}{Z_0} - \frac{1}{Z_0} - \cdots \right)^{-1} - \left(\frac{1}{Z_0} - \frac{1}{Z_0} - \cdots \right) \right]^{-1} \tag{28}$$

or

$$\beta G^\infty(n) = (t^{-1} - t)^{-1} \tag{29}$$

where

$$t = \frac{1}{Z_0} - \frac{1}{Z_0} - \cdots = \frac{1}{Z_0 - t} \tag{30}$$

so that

$$t^2 - 2Xt + 1 = 0 \tag{31}$$

whose roots are given by

$$t_\pm = X \pm (X^2 - 1)^{1/2} \qquad t_+ t_- = 1. \tag{32}$$

With the aid of (32), substituting (30) into (29) leads to

$$\beta G^\infty(n) = -\left[2i(1 - X^2)^{1/2} \right]^{-1} \tag{33}$$

as required for the $F = 0$ case [20]. When $n = 0$ in (27), we obtain

$$\begin{aligned} \beta G^\infty(0) = \Bigg[&\left(\frac{1}{Z_0} - \frac{1}{Z_{-1}} - \cdots \frac{1}{Z_{-N}} - \cdots \right)^{-1} \\ &- \left(\frac{1}{Z_1} - \frac{1}{Z_2} - \cdots \frac{1}{Z_N} - \cdots \right) \Bigg]^{-1} \end{aligned} \tag{34}$$

which by (26) can be written as

$$\beta G^{\infty}(0) = -\frac{J_{\nu}(x)J_{-\nu}(x)}{J_{\nu+1}(x)J_{-\nu}(x) + J_{\nu}(x)J_{-\nu-1}(x)}. \tag{35}$$

However, the denominator in (35) is the *Wronskian* [22]

$$W[J_{\nu}(x), J_{-\nu}(x)] = -2\sin\nu\pi/\pi x \tag{36}$$

so (35) reads

$$\beta G^{\infty}(0) = \frac{\pi x J_{\nu}(x)J_{-\nu}(x)}{2\sin\nu\pi}. \tag{37}$$

3. Density of states

Having found the GFs for the three cases in question, we can now obtain their *local density of states* (LDOS) at the site n via the usual formula [20]

$$\rho_n(X) = \pi^{-1}\mathrm{Im}\, G(n; X). \tag{38}$$

Since $G(n; X)$ is *real valued everywhere*, only at the reduced eigenenergies, $X = X_k$, will the imaginary component be admitted, the X_k-values being provided by the *poles* of the GF. Invoking the *theory of residues* [23], we arrive at

$$\mathrm{Im}\, G(n; X_k) = \pi/(\beta\left[\Lambda(X_k)^{-1}\right]') \tag{39}$$

where the prime denotes differentiation with respect to X (i.e. *order* ν by (24)), and $\Lambda(X) = \beta\mathrm{Re}\, G(n; X)$. Using (39), we can express (38) as

$$\rho_n(X) = \sum_k I_k^n(X_k)\delta(X - X_k)/(2\beta) \tag{40}$$

where

$$I_k^n(X_k) = 2\left\{[\Lambda(X_k)^{-1}]'\right\}^{-1} \tag{41}$$

is the *intensity energy distribution* at the atom n, which can also be interpreted as the electron *occupation number* of the state k. We are now in a position to address the LDOS for the above cases separately.

3.1. Finite chain

The plots of the LDOS at the $n = 0$ site of a 100-atom chain are presented in figure 2 for the various fields indicated. The intensities, $I_k^0(X_k)$, in (41) were obtained by using the exact rational polynomial form of (25), which can be derived from the Wronskian equations for both numerator and denominator, where the reduced energies, X_k, are provided by the poles of (25), i.e. the solutions of

$$J_{\nu_k-1}(x)Y_{\nu_k+N}(x) - J_{\nu_k+N}(x)Y_{\nu_k-1}(x) = 0. \tag{42}$$

Figure 2(a) depicts the *discretized* form of the familiar semi-elliptic LDOS for the zero-field case [20]. On applying the small field $F = 0.005$, the band picture of figure 2(b) arises, in which the most striking feature is the appearance of the *linear-ramp* WS-region of negative slope covering the lower quarter of the band. In addition, the band is rigidly shifted slightly to higher energies, the intensities decaying exponentially beyond the upper-band edge at $X = 1$. Note also the redistribution of the X_k-values compared with those in figure 2(a). Increasing the field to $F = 0.01$, the WS-region in figure 2(c) now extends over *all* the lower half of the band, and about half its intensities exceed the maximum of those

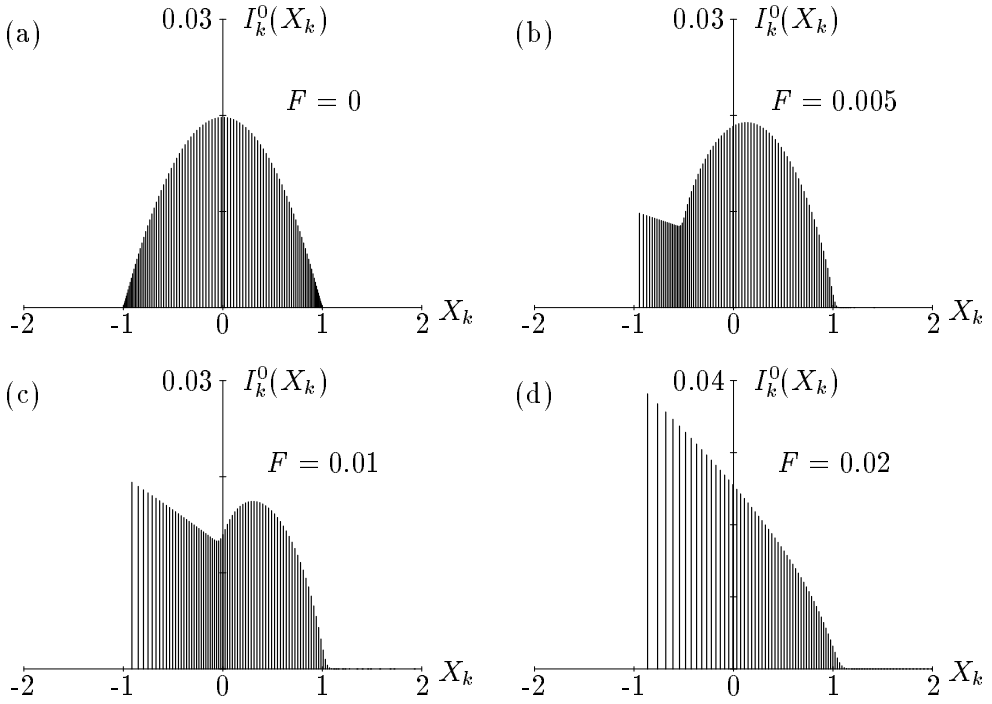

Figure 2. LDOS at $n = 0$ site of 100 atom chain. As field increases, semi-elliptical shape is dominated by linear field. Field strengths are as indicated.

in the semi-elliptic portion. Doubling the field to $F = 0.02$, the WS-region *completely* supersedes the semi-elliptic one, as in figure 2(d), and is again accompanied by the rigid shift to higher X_k-values and the exponential tailing above $X = 1$. Moreover, the $I_k^0(X_k)$ values are markedly larger than those in the $F = 0$ situation in figure 2(a), particularly in the lower half of the WS-band. Note here, and elsewhere, that $\sum_k I_k^n(X_k) = 1$ regulates the heights of the intensity spikes. In the case of F *negative*, the corresponding LDOS plots are those of figure 2, reflected in the $X_k = 0$ vertical axis.

3.2. Semi-infinite chain

Here, we use (26) in (39) and (41), with $n = 0$, to obtain

$$I_k^0(X_k) = 2x^{-1}J_{\nu_k}(x)[J'_{\nu_k-1}(x)]^{-1} \tag{43}$$

the X_k-values being the solutions of

$$J_{\nu_k-1}(x) = 0 \tag{44}$$

i.e. the poles of (26).

In contrast to the finite and infinite chains' LDOS plots at the $n = 0$ site, here we are concerned with the LDOS at a *number* of sites in the chain, when the field is *fixed* at $F = 0.02$. Starting at the end site, $n = 0$, we immediately see that figure 3(a) essentially replicates that of figure 2(d), for this site of the finite chain under the same field. Moving to the next site at $n = 1$, figure 3(b) shows that a drastic change has occurred in the LDOS, at this first *subsurface* atom. The distinct features are the extremely high spike at the lower-band edge followed by a steep decline to $I_k^0(0) = 0$ over the bottom half of the WS-band,

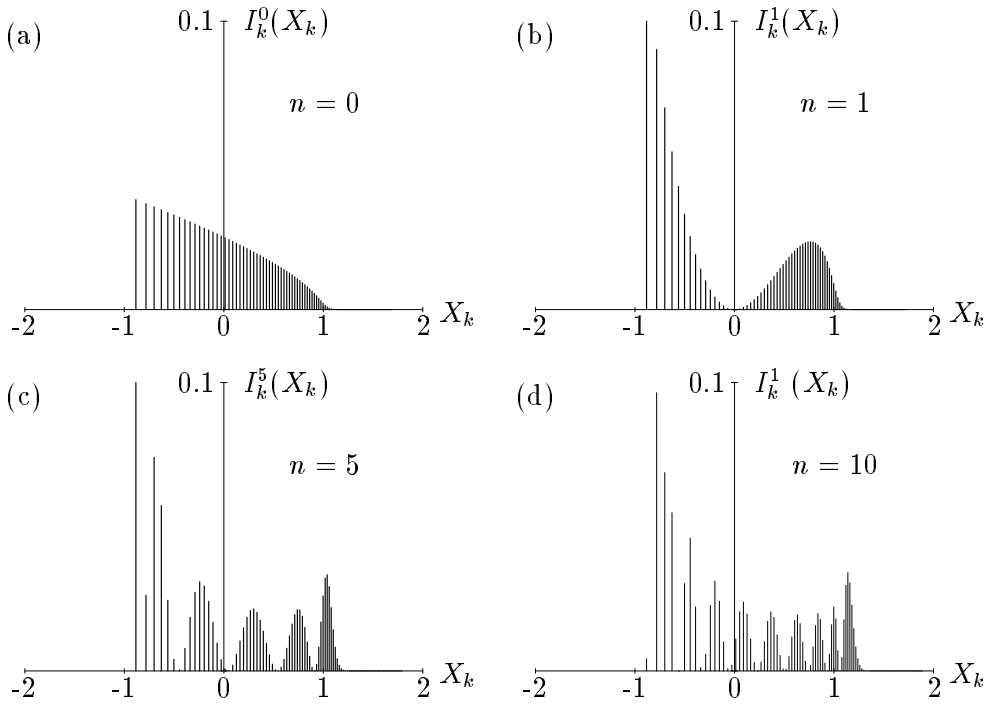

Figure 3. Transition from surface ($n = 0$) to bulk ($n = 10$) LDOS of semi-infinite chain subject to a linear applied field of $F = 0.02$. Site positions are as shown.

while in the top half we witness the emergence of the first *bulk* contribution in the form of a *discretized hump*. Penetrating the chain further, to the $n = 5$ site, figure 3(c) displays a *series of spike clusters of Gaussian-like* (GL) *shape*, except at the lower-band edge, where the dominant spike is again present. We also notice that the envelope through the GL peak maxima takes on the familiar U-shape of a bulk LDOS. The $I_k^{10}(X_k)$ plot of figure 4(d) is for the *bulk* site at $n = 10$. As in figure 4(c), we find a series of GL peaks, each separated by a *node* (i.e. $I_k^{10}(X_k) = 0$). The number of nodes (and peaks) increases with n. Note that the bulk character of this LDOS is reflected in the disappearance of the dominant spike at the lower-band edge, which is connected with the *surface state* [20] associated with the end atom at $n = 0$. The U-shape envelope is, of course, still retained and the band tailing at the upper-band edge has become more pronounced, in conjunction with the rigid shift of the WS-band, as n increases.

3.3. Infinite chain

From (37) and (41), we find that

$$I_k^0(X_k) = \sec(\nu_k \pi) J_{\nu_k}(x) J_{-\nu_k}(x) \tag{45}$$

the poles of (37) providing the X_k-values, viz,

$$\sin \nu_k \pi = 0 \tag{46}$$

i.e.

$$X_k = kF \qquad k = 0, \pm 1, \pm 2, \ldots \tag{47}$$

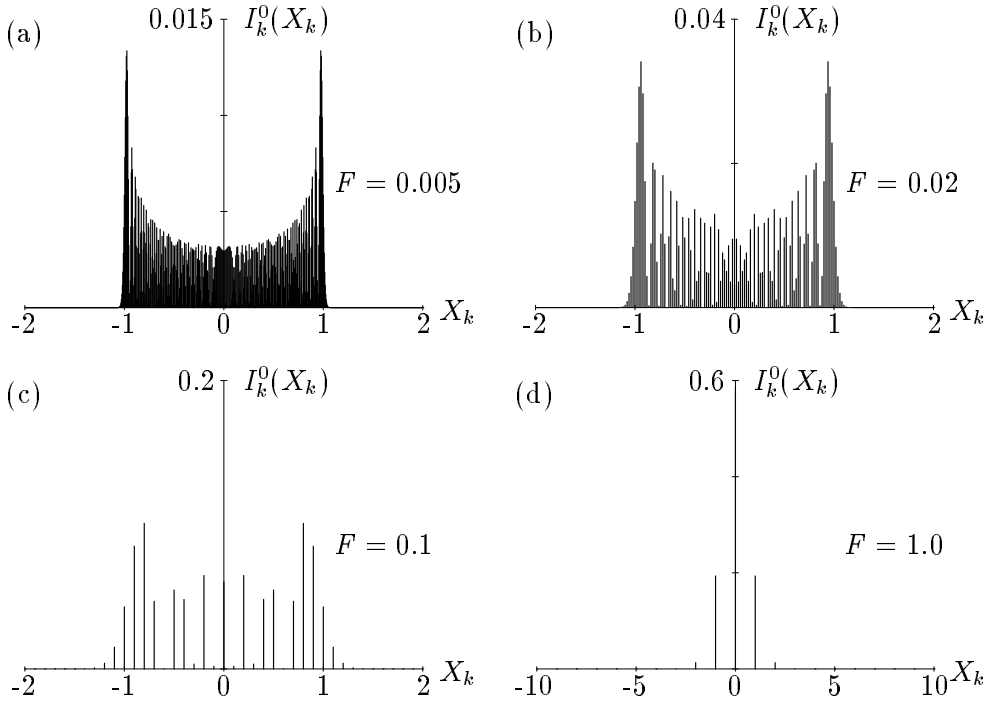

Figure 4. Occupation number of states for infinite chain. Continuous field transition from discretized U-shape of zero-field to the localized peak for $F \geqslant 1$ occurs by combining both U and GL features into multiple Stark ladders. Field strengths are as indicated.

by (24). Thus $\nu_k = -k$, and so

$$\sec(\nu_k \pi) = (-1)^k = (-1)^{\nu_k}. \tag{48}$$

Since $J_{-\nu}(x) = (-1)^{\nu} J_{\nu}(x)$ [22], it follows from (23) that $I_k^0(X_k)$ in (45) varies as the probability, $|c_k^0|^2$, giving the link to the k-state occupation number at the zero atom. Note, (47) defines a *true* WSL, in contrast to the *quasi*-WSLs given by the BF conditions in (42) and (44).

The LDOS are shown in figure 4 for the F-values indicated. The low-field ($F = 0.005$) case of figure 4(a) has the U-shape appearance of the $F = 0$ situation [20], and the *discrete details* are reminiscent of the $\Gamma = 0.01$ plot of the *ground-state profile* obtained numerically by Dolcher *et al* [16], including the band tailing at *both* band edges. For $F = 0.02$, in figure 4(b), the *fine structure* of the discrete details is resolved, showing the intensity spikes are again clustered into energy regions, which we identify as the break-up of the *single* WS-band into the *multiple mini-WS-bands* and were suggested by Moyer [15] as a means of approaching the zero-field limit in a proper manner. Further increase of the field to $F = 0.1$ results in figure 4(c), where the heights of the intensity spikes are greatly diminished and their separation and band tailing greatly enhanced, making the characteristic U-shape barely discernible. Taking the field to $F = 1.0$, the WS-band structure is reduced to that in figure 4(d), whose few spikes form a *single* GL distribution about the central dominant spike at $X_k = 0$, the U-shape being completely destroyed. Conversely, the single GL peak can be regarded as the *basic unit* from which the other WS spectra are generated.

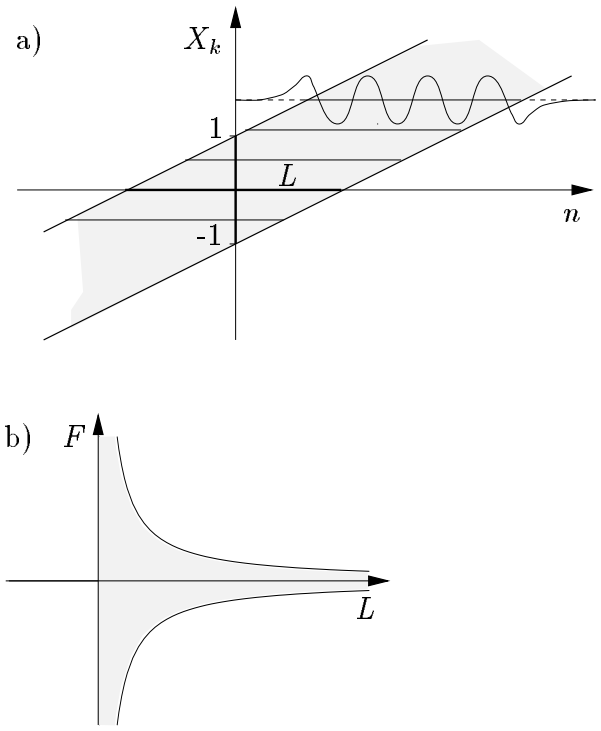

Figure 5. (a) WS-band showing localization length L and wavefunction behaviour. (b) Rectangular hyperbolae $FL = \pm 2$ bounding shaded region in which (F, L) values give rise to band state.

Let us now address the question of the *number* of states in the WS-band at a given field strength. The *tilted band picture* of the WSL (47) is shown in figure 5(a), where X_k vs. n is drawn. The *upper* (*lower*) band edge is the line $X_k = n + 1$ ($X_k = n - 1$). Between these lines, the vertical (horizontal) bandwidth is 2 (L), L being the so-called *localization length*, over (beyond) which the BF is oscillatory (damped exponentially). From the geometry of figure 5(a), we see that the field gradient $F = \pm 2/L$, or $|FL| = 2$. Thus, for a state to be *in* the band, the *rectangular hyperbolic condition* (figure 5b)

$$|FL| \leqslant 2 \tag{49}$$

must be satisfied. Since, in the one-electron approximation, each chain atom contributes one state, the actual number of states in the WS-band corresponds to the number over which L ($= 2F^{-1}$) extends. Hence, when $F = 1$, $L = 2$ and the number of states supported by the WS-band at $n = 0$ is *three*, as in figure 4(d), where the band-tailing states beyond the edges are *neglected*. Reducing F to 0.1 (figure 4c), we find *21 states* in the band, corresponding to $L = 20$. Whence, in general, the number of states in the WS-band is

$$N = 2\left[L/2\right] + 1 = 2\left[1/|F|\right] + 1 = 2\left[|x|\right] + 1 \tag{50}$$

where the square brackets indicate the integer part of the argument.

Finally, we should mention that the methodology described herein has been applied to the study of the WS effect on surface states [24] and chemisorption [25].

4. Conclusion

The effect of an applied electric field on TB systems has been investigated by means of the RGF approach, which provided access to the LDOS. By invoking Pincherle's theorem, the continued-fraction form of the RGF was expressed *analytically* as the ratio of Bessel functions, in contrast to the previous numerical treatments [16]. LDOS results were presented for finite, semi-infinite and infinite TB systems, for various field strengths.

The poles of the RGFs provided the energy-level values, at which the LDOS was evaluated, via the imaginary part of the RGF. The presence of the energy Dirac δ-function in the LDOS expression gives rise to the *discrete* nature of the LDOS, so the spectrum shows none of the field-induced broadening usually associated with such interactive systems. This outcome is perhaps not too surprising, in view of the fact that the applied field destroys the translational symmetry of the crystal, so that each atom is distinguished by a different site energy. Thus, the system has ostensibly become a linear array of *impurity* atoms, each supporting a localized state with a discrete energy level. It should be pointed out, however, that the TB approach neglects the scattering states of the atoms which, if included, would lead to a *smooth* (rather than discrete) spectrum with eigenstates decaying algebraically in the region of large, negative electronic potential energy.

With increasing field strength, the LDOS envelope at the *end atom* exhibits a competition between the familiar semi-elliptic shape and the linear-ramp WS shape, accompanied by a redistribution of the reduced-energy levels. Moving to an atomic site *inside* the chain reveals the emergence of an oscillatory behaviour in the LDOS envelope, with the number of nodes corresponding roughly to the distance from the end atom. At an atomic site in the *bulk*, where the energy levels form a regular WSL, the oscillatory shape breaks-up into a number of WS mini-bands, with the familiar U-shape appearance at low fields and just a few dominant spikes at high fields. In particular, the seemingly irregular discrete details of the LDOS in the bulk are reminiscent of the numerical findings of Dolcher *et al* [16].

In the present one-band TB treatment, degeneracy does not arise, because the system in question is considered to be *isolated*. However, on connecting it to the outside world via leads, the levels in the applied-field region would become degenerate with those in the leads, thus providing a channel for electron transport. In the case of electrified semiconductors, the levels in the valence and conduction bands are degenerate, and charge transfer across the band gap occurs by Zener tunnelling.

The methodology formulated here can be extended to two- and three-dimensional systems, in the manner of Pendry *et al* [19]. It is also applicable to electrified superlattices, and should be a useful aid in designing atomic-switching devices, which are currently being fabricated by scanning-tunnelling microscopes [26].

Acknowledgments

The work reported here was supported by the Natural Sciences and Engineering Research Council (NSERC) of Canada and the North Atlantic Treaty Organization. One of the authors (SGD) also wishes to thank the Royal Society of London and NSERC for the award of a grant under the auspices of the Bilateral-Exchange Scheme.

References

[1] Zener C 1934 *Proc. R. Soc (London)* **145** 523
[2] Wannier G H 1960 *Phys. Rev.* **117** 432

[3] Wannier G H 1962 *Rev. Mod. Phys.* **34** 645
Zak J 1968 *Phys. Rev. Lett.* **20** 1477
Zak J 1972 *Solid State Physics* vol 27 ed F Seitz *et al* (New York: Academic) pp 1–61
Avron J E, Zak J, Grossman A and Gunther L 1977 *J. Math. Phys.* **18** 918
Churchill J N and Holmstrom F E 1982 *Am. J. Phys.* **50** 848
[4] Hacker K and Obermair G 1970 *Z. Phys.* **234** 1
Fukujama H, Bari R and Fogedby H C 1973 *Phys. Rev.* B **8** 5579
Saito M 1973 *J. Phys.* C **6** 3255
Richardson M J and Davison S G 1974 *Can. J. Phys.* **52** 2395
Leo J and McKinnon A 1989 *J. Phys.: Condens. Matter* **1** 1449
[5] Zhao X G 1991 *J. Phys.: Condens. Matter* **3** 6021
Zhao X G 1991 *Phys. Lett.* **A154** 275
[6] Zhao X G 1992 *Phys. Lett.* **A167** 391
[7] Ahn D 1993 *Phys. Rev.* B **48** 7981
[8] Anwar A F M and Jahan M M 1994 *Phys. Rev.* B **50** 10864
[9] Vrubel M M and Borzdov V M 1995 *Physica* B **215** 201
[10] Sari H, Metin H, Sökmen I, Elagöz S and Ergün Y 1995 *Superlat. Microst.* **17** 457
[11] Cohen G, Bar-Joseph I and Shtrikman H 1994 *Phys. Rev.* B **50** 17316
[12] Kavaliauskas J, Kivaitė G, Galickas A, Šimkienė I, Olin U and Ottosson M 1995 *Phys. Status Solidi* b **191** 155
[13] Lukes T and Somaratna K T S 1969 *J. Phys.* C **2** 586
Lukes T and Somaratna K T S 1969 *Phys. Lett.* **A29** 69
Lukes T and Morgan D J 1973 *Phys. Status Solidi* b **57** K47
[14] Feynman R P and Hibbs A R 1965 *Quantum Mechanics and Path Integrals* (New York: McGraw-Hill)
[15] Moyer C A 1973 *Phys. Rev.* B **7** 5025
[16] Dolcher V, Grosso G, Martinelli L and Parravicini G P 1996 *Phys. Rev.* B **53** 10 813
[17] Gvozdikov V M 1996 *Phys. Rev.* B **53** 10 133
[18] Haydock R 1980 *Solid State Physics* vol 35 ed F Seitz *et al* (New York: Academic) pp 215–94
[19] Pendry J B, Prêtre A, Rous P J and Martín-Moreno L 1991 *Surf. Sci.* **244** 160
[20] Davison S G and Stęślicka M 1992 *Basic Theory of Surface States* (Oxford: Clarendon)
[21] Lorentzen L and Waadeland H 1992 *Continued Fractions with Applications* (Amsterdam: North-Holland)
[22] Olver F W J 1972 *Handbook of Mathematical Functions* ed M Abramowitz and I A Stegun (Washington DC: US Department of Commerce)
[23] Priestley H A 1985 *Introduction to Complex Analysis* (Oxford: Oxford University Press)
[24] English R A, Davison S G, Mišković Z L, Goodman F O, Amos A T and Burrows B L 1996 *Prog. Surf. Sci.* **53** 323
[25] English R A, Davison S G, Mišković Z L, Goodman F O, Amos A T and Burrows B L 1997 *Prog. Surf. Sci.* **54** 241
[26] Wada Y, Uda T, Lutwyche M, Kondo S and Heike S 1993 *J. Appl. Phys.* **74** 7321
Kaetter E, Drakova D and Doyen G 1996 *Phys. Rev.* B **53** 16 595
Gao S, Persson M and Lundquist B I 1997 *Phys. Rev.* B **55** 4825